JOURNAL OF MATERIALS SCIENCE 19 (1984) 1851–1862

Stress relaxation in bending of type AISI 304 and A-286 steels at 773 K

F. POVOLO
Comisión Nacional de Energía Atómica, Dto. de Materiales. Av. del Libertador 8250, (1429) Buenos Aires, Comisión de Investigaciones Científicas de la Provincia de Buenos Aires, Argentina

R. TINIVELLA
Universidad Tecnológica Nacional, Facultad Regional S. Nicolás, (2900) S. Nicolás, Argentina

Stress relaxation measurements at 773 K, in bending and for different initial stresses, in Type AISI 304 and A-286 steels are reported. Several thermomechanical treatments were given to the specimens prior to the relaxation testing. The data are interpreted in terms of a stress-partitioned power law and it is shown, for AISI 304, that, for certain thermomechanical treatments, the internal stress depends on the applied stress since the microstructure recovers during the relaxation.

1. Introduction

Conway *et al.* [1] have reviewed the stress relaxation behaviour of stainless steels for data analysed in a stress against time diagram. Rhode and Swearengen [2] considered the load relaxation data reported by Conway [3], for 304 and 316 stainless steels during cyclic deformation and various hold times, for experiments conducted at 923 K and 811 K. The stress relaxation curves were analysed in a stress against strain rate diagram by using the relationship

$$\dot{\epsilon}/\dot{\epsilon}_1 = \left\{(1-A)\left[\frac{\sigma-\sigma_i}{\sigma_1}\right]^{m/n} + A\left[\frac{\sigma-\sigma_i}{\sigma_1}\right]\right\}^n \quad (1)$$

where σ is the applied stress, $\dot{\epsilon}$ the plastic strain rate, m is a state variable that relates dislocation velocity to stress, n is a state variable that denotes the recovery rate, the state parameter σ_i is an internal stress which becomes zero at high temperatures and A is a functional relationship between m,n, strain hardening and recovery. σ_1 and $\dot{\epsilon}_1$ are the stress and strain rate, respectively, at the beginning of the relaxation.

In 304 and 923 K it was found that short hold times and large cyclic strain amplitudes inhibit recovery. Conversely, long hold times and small cyclic strains promote recovery. When recovery occurs, relaxation can be described with $\sigma_i = 0$, $m \simeq 40$ and $n \simeq 10$. If no recovery occurs $\sigma_i \neq 0$ and $m \simeq 3$. At 811 K for 304 no evidence of recovery was found and $\sigma_i \neq 0, m \simeq 2.5$.

Anciaux [4] reported stress relaxation curves for three austenitic stainless steels at 563 K. The tests were conducted in a strain controlled servo-hydraulic test machine near yield point strain levels. The shape of the stress–strain rate trajectories for the mill-annealed Type-304 stainless steel were found to be dependent on the applied strain. No explanation was given for this behaviour.

The state variable approach proposed by Hart [5, 6] was used by several authors [7–14] to describe the load relaxation behaviour of Type-304 and Type-316 stainless steels. Hart's phenomenological model consists of essentially two parallel branches. At high homologous temperatures the constant hardness log σ–log $\dot{\epsilon}$ stress relaxation curves are described by

$$\ln(\sigma^*/\sigma) = (\dot{\epsilon}^*/\dot{\epsilon})^\lambda \quad (2)$$

where σ^* is the hardness, λ is a temperature-independent parameter and $\dot{\epsilon}^*$ depends on temperature, heat treatment and deformation. The rate

0022–2461/84 $03.00 + .12

of deformation in the region where Equation 2 applies is assumed to be controlled by diffusive processes.

The branch which is important at lower homologous temperatures gives the constant hardness log σ–log $\dot{\epsilon}$ curves described by

$$\dot{\epsilon} = B(\sigma_f/G)^M \quad (3)$$

where G is the shear modulus, B is a rate parameter and is moderately temperature dependent compared to $\dot{\epsilon}^*$, σ_f is an effective stress and is $(\sigma - \sigma^*)$ in the region where deformation processes represented by Equation 2 are not important and M is a constant. Equation 3 is assumed to result from dislocation glide controlled processes.

In the intermediate temperature range, deformation processes represented by both Equations 2 and 3 will be important. In this range both branches of the phenomenological model will be operative such that

$$\sigma = \sigma^* \exp[-(\dot{\epsilon}^*/\dot{\epsilon})^\lambda] + G(\dot{\epsilon}/B)^{1/M} \quad (4)$$

Most of the data were obtained at room temperature and have been interpreted in terms of Equation 3. It was found that the parameters of Equation 3 were dependent on the prior thermomechanical treatment given to the specimen [7, 10]. The measurements in Type-316 stainless steel were extended to higher temperatures [12, 14] and could be described by Equation 4 up to temperatures of the order of 773 K. Microstructural changes were observed above this temperature. A grain-boundary sliding contribution to the relaxation curves was observed at 873 K, in a highly stabilized Type-316 stainless steel [14]. This contribution was described by an equation similar to Equation 2 with $\lambda = 0.32$.

The only data found in the literature on the stress relaxation of Type A-286 stainless steel are those reported by Matters and Lochen [15] for springs at constant deflection. The experiments were performed at 811 and 922 K for only one initial stress and up to times of the order of 500 h. These data are largely qualitative and were obtained in aged material.

It is the purpose of this paper to present data on the stress relaxation behaviour, in bending and at 773 K, of Type A-286 and 304 stainless steels. Four different thermomechanical treatments are given to the specimens, prior to the stress relaxation experiments and the measurements are extended up to times of 350 h at various initial stresses.

2. Experimental procedure

2.1. Specimen's preparation

The as received material was cold-rolled to the desired thickness (of the order of 0.5 mm) to prepare specimens 15 mm wide and 100 mm long. This, produced a 30% deformation in the A-286 and 50% in the AISI 304 specimens, respectively. The specimens were prepared with the axis parallel to the rolling direction and, in addition to the cold-worked condition, three different thermal treatments were used, prior to the stress relaxation measurements. In fact, some specimens were carefully cleaned and sealed into fused silica tubes with argon atmosphere. These tubes were heated during 1 h either at 1172 K or at 1201 K and dropped into oil for a quenching treatment. Finally, the specimens were heat-treated into a fused silica tube connected to a high vacuum equipment, at 993 K during 16 h and subsequently cooled by removing the furnace ("air cooling"). These different thermomechanical treatments will be named A, B, C and D, respectively, as indicated in Table I. The chemical composition of both alloys, the average grain size and the microhardness obtained after the different thermomechanical treatments are indicated in Table II.

2.2. Stress relaxation measurements

The specimens, originally flat, were bent elastically into stainless steel holders with radii which gave maximum outer fibre stresses between approximately 100 and 300 MPa. The holders are similar to those described by Fraser *et al.* [16]. The holders with the specimens were inserted into a furnace at 773 K and extracted periodically for curvature measurements. The temperature was controlled with thermocouples attached to the holders near the specimens and the fluctuations

TABLE I Thermomechanical treatments given to the specimens prior to the stress relaxation tests

Thermomechanical treatment	Name
As-received + cold-rolled	A
A + 16 h at 993 K in vacuum and "air-cooled"	B
A + 1 h at 1172 K in argon and oil-quenched + 16 h at 993 K in vacuum and "air-cooled"	C
A + 1 h at 1201 K in argon and oil-quenched + 16 h at 993 K in vaccum and "air-cooled"	D

TABLE IIA Chemical composition of the alloys used.

	Composition (wt %)													
	C	Mn	P	S	Si	Cr	Ni	Mo	Co	V	Ca	Al	Ti	Fe
AISI 304	0.058	1.7	0.020	0.012	0.75	17	8.8	0.27	0.08	0.05	–	–	–	balance
A-286	0.042	< 0.1	0.025	0.037	< 0.1	14	25	2.02	0.85	0.52	0.025	1.13	2.10	balance

TABLE IIB Thermomechanical treatment

	Thermomechanical treatment (Average grain size (μm); microhardness (HV))			
	A	B	C	D
AISI 304	45; 450	37; 209	11; 225	35; 215
A-286	45; 366	41; 497	19; 374	28; 334

were of the order of ± 1 K. The radii of curvature, R_i, after releasing the specimens from the holders were determined by measuring the coordinates of different points with respect to a reference plane, in the arc of circumference determined by the curved beam and feeding the data to a computer program which calculated the average radius by a least squares fitting. Duplicate specimens were used in order to observe the dispersion between equivalent specimens on the results. The stresses at the surface of the beam, σ, before unloading were determined by the relationship [17, 18]

$$\sigma = \tfrac{2}{3}\sigma_b + \frac{\Sigma}{3}\frac{d\sigma_b}{d\Sigma} \qquad (5)$$

where $\Sigma = Eh/2R$ is the initial stress at the surface of the bent specimen and

$$\sigma_b = (Eh/2)\left(\frac{1}{R_i} - \frac{1}{R}\right)$$

the measured stress change in the same position, after releasing the specimen from the holder. R is the radius of curvature of the holder, h is the thickness of the specimen and E is Young's modulus (168 GPa for AISI 304 [19] and 167 GPa for A-286 [20] at 773 K, respectively).

3. Results

3.1. A-286

Fig. 1 shows the measured stress change at the surface of the specimens, for different thermomechanical treatments and various initial stresses.

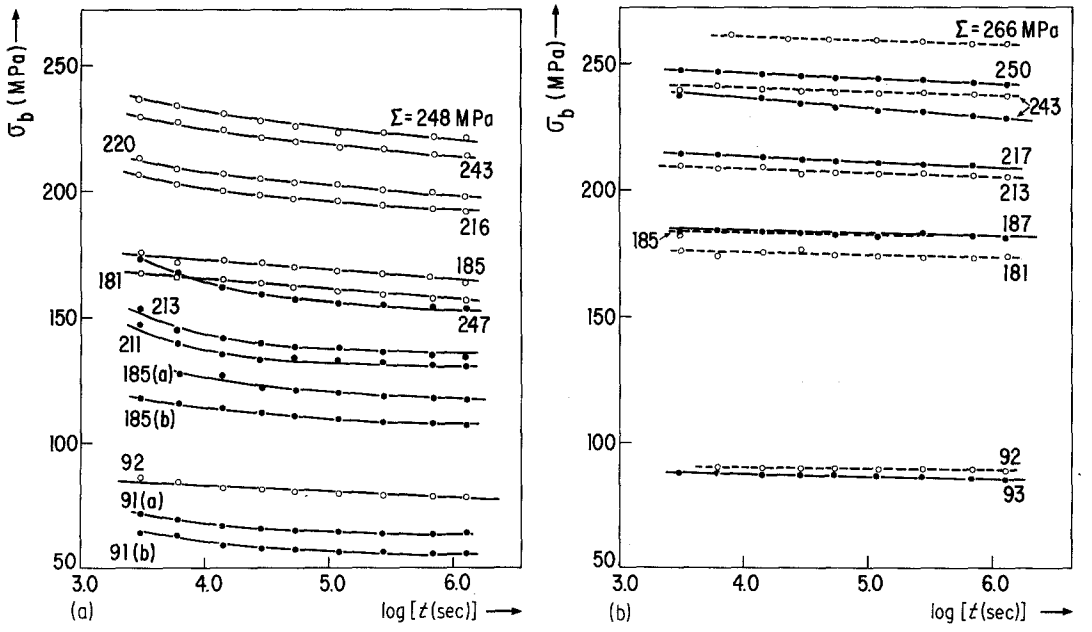

Figure 1 Measured stress change at the surface as a function of time for A-286. (a) The full circles correspond to specimens Type-A and the open circles to specimens Type-B, respectively. (b) The full curves indicate specimens Type-C and the broken curves specimens Type-D, respectively. The corresponding initial stresses are given on each curve.

It is seen that in some cases, for example the full curves for $\Sigma = 91$ MPa at the bottom of Fig. 1a equivalent specimens can give slightly different results (curve 91(a) and curve 91(b)). This is due to the fact that, even if both specimens had the same thermomechanical treatment, there might be a slight difference in the initial state of the material. Small differences in the thickness of the specimens are indicated by curves with slight differences in the initial stresses as, for example, the full curves for $\Sigma = 213$ MPa and $\Sigma = 211$ MPa in Fig. 1a. When only one curve is shown, for a given Σ, the data correspond to the average value for two equivalent specimens. The stresses, σ, at the surface of the specimen before unloading, which correspond to the values that would be obtained, in the same material, under initial uniaxial stresses given by Σ, can be calculated by using Equation 5. In fact, $d\sigma_b/d\Sigma$ can be obtained by plotting σ_b against Σ for different times and drawing average curves through the points obtained from the average curves of Fig. 1. Once $d\sigma_b/d\Sigma$ is known, at each t, curves of σ against t can be easily constructed. These curves are not given to save space.

The $\log \sigma$–$\log \dot{\epsilon}$ stress relaxation curves are obtained by taking the derivatives of the σ against t curves, since $\dot{\epsilon} = -\dot{\sigma}/E$; the dot indicates a derivative with respect to the time. These curves are shown in Fig. 2 where the same notation as for Fig. 1 is used. It is seen that the cold-worked specimens (Type A) show a higher stress relaxation as compared with treatments B, C and D.

The stress relaxation curves for the cold-worked specimens are concave upward as for a typical process at low homologous temperatures [5, 6, 21]. A visual comparison of these curves with the normalized plots of the different theoretical expressions [22] shows that these data might be described either by Gilman's [23] equation, by a hyperbolic sine relationship between the average dislocation velocity and the effective stress, or by the Johnston–Gilman [24] equation. This last equation is similar to Equation 3.

The best fit to the experimental curves for the cold-worked specimens shown in Fig. 2a was obtained with the Johnston–Gilman equation. The following procedure was used [25]: Johnston–Gilman equation

$$\dot{\epsilon} = \phi\rho\mathbf{b}v_0\left[\frac{\sigma - \sigma_i}{\sigma_0}\right]^{m^*} \tag{6}$$

where ϕ is an orientation factor, ρ is the mobile dislocation density, $\mathbf{b}$ is the Burgers vector, σ_i is an internal stress and, v_0, σ_0 and m^* are material constants, can be written in a normalized form as [22]

$$\alpha\sigma = 1 + (\dot{\epsilon}/\dot{\epsilon}^*)^{1/\beta} \tag{7}$$

where

$$\dot{\epsilon}^* = \phi\rho\mathbf{b}v_0(\sigma_i/\sigma_0)^{m^*} \tag{8}$$

$$\beta = m^* \tag{9}$$

$$\alpha = 1/\sigma_i \tag{10}$$

The strain rate sensitivity parameter $\nu = d\log\sigma/d\log\dot{\epsilon}$, obtained by differentiating Equation 7, is given by [22]

$$\nu = (\dot{\epsilon}/\dot{\epsilon}^*)^{1/\beta}/[1 + (\dot{\epsilon}/\dot{\epsilon}^*)^{1/\beta}]\beta \tag{11}$$

Combining Equations 7 and 11 leads to

$$\sigma = (1/\alpha) + \beta(\sigma\nu) \tag{12}$$

Equation 12 shows that, if the experimental

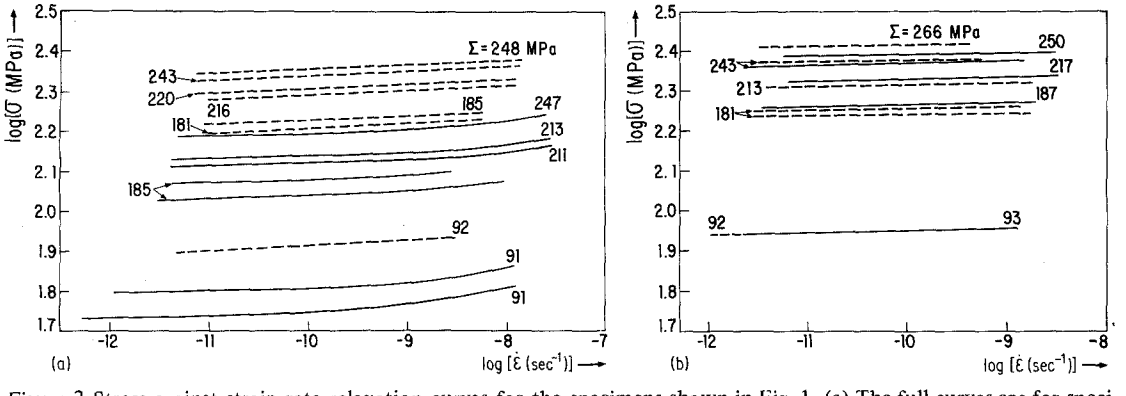

Figure 2 Stress against strain rate relaxation curves for the specimens shown in Fig. 1. (a) The full curves are for specimens Type-A and the broken curves for specimens Type-B, respectively. (b) The full curves indicate specimens Type-C and the broken curves specimens Type-D, respectively.

TABLE III Parameters for the A-286 cold-worked specimens, Type-A, obtained by fitting the experimental log σ–log $\dot{\epsilon}$ curves of Fig. 1a to Johnston–Gilman equation

Σ (MPa)	$\sigma_i = 1/\alpha$ (MPa)	m^*	$\dot{\epsilon}^*/\sigma_i^{m^*} = \phi\rho b v_0/\sigma_0^{m^*} \times 10^{11}$ (sec^{-1} MPa^{-m^*})	$\alpha(\dot{\epsilon}^*)^{1/m^*} \times 10^3$ (sec^{-1/m^*} MPa^{-1})
247	157	2	7.6	8.7
213	136.2	2	9.1	9.5
185(a)	109	2	9.4	9.7
91(a)	62.9	2	7.2	8.5

curves are described either by Equations 6 or 7, a plot of the derivative of the log σ–log $\dot{\epsilon}$ curves multiplied by the corresponding stress against the stress should give a straight line of slope β and intercept $1/\alpha$. Once α and β are known, $\dot{\epsilon}^*$ can be obtained from Equation 7.

Equation 12 was applied to the experimental log σ–log $\dot{\epsilon}$ curves for the cold-worked specimens, shown in Fig. 2a and the parameters obtained are given in Table III. It must be pointed out that the experimental curves shown in Fig. 2a, for Type-A specimens, can be fitted with the parameters given in Table III with a maximum error of the order of 1%. As shown in Fig. 2, specimens Type-B, C and D give a straight line in a log σ–log $\dot{\epsilon}$ plot. From Equations 7 and 11 it is easily seen that if $\alpha\sigma \gg 1$, then

$$\alpha\sigma = (\dot{\epsilon}/\dot{\epsilon}^*)^{1/\beta} \quad (13)$$

and

$$\nu = 1/\beta \quad (14)$$

TABLE IV Parameters for the A-286 specimens Type-B, C and D obtained by fitting the data of Fig. 2 to Equation 15

Specimen type and m^*	Σ (MPa)	$\alpha(\dot{\epsilon}^*)^{1/m^*} \times 10^3$ (sec^{-1/m^*} MPa^{-1})
B	248	3.3
$m^* = 76.9$	243	3.4
	220	3.7
	216	3.8
	185	4.5
	181	4.6
	92	9.0
C	250	3.7
$m^* = 222.2$	243	3.9
	217	4.2
	187	4.9
	93	10.0
D	266	3.8
$m^* = 266.7$	243	4.1
	213	4.7
	185	5.4
	181	5.5
	92	10.3

On taking the logarithm of both sides of Equation 13 and rearranging gives

$$\log\sigma = -\log[\alpha(\dot{\epsilon}^*)^{1/\beta}] + (\log\dot{\epsilon}/\beta) \quad (15)$$

which shows that a plot of log σ against log $\dot{\epsilon}$ should be linear with a slope $1/\beta$ and intercept $-\log[\alpha(\dot{\epsilon}^*)^{1/\beta}]$. The parameters obtained by applying Equation 15 to specimens Type-B, C and D are given in Table IV.

3.2. AISI 304

Fig. 3 shows the measured stress change at the surface of the specimens for the different thermomechanical treatments and various initial stresses. The average value obtained in two equivalent specimens is given. The strong relaxation in the cold-worked specimens should be noticed.

The corresponding log σ–log $\dot{\epsilon}$ stress relaxation curves, obtained through a procedure similar to the one used for the A-286 specimens, are shown in Fig. 4. It is seen that in this case concave upward or concave downward curves can be obtained, according to the thermomechanical treatment. Specimens Type-A and D give concave upward curves which can be described by the Johnston–Gilman equation (Equation 6) following the procedure outlined for the A-286 specimens. The corresponding parameters are given in Table V and the experimental curves can be fitted to Equations 6 or 7 with a maximum error of 1%.

A visual comparison of the concave downward curves of Fig. 4 for specimens Type-B and C, with the normalized plots of [22] shows that these curves might be described either by an exponential dependence of the strain rate with the applied stress, by a hyperbolic sine dependence of the strain rate with the applied stress, by Sleeswyk *et al.* [26] model or by Hart's phenomenological model for high homologous temperatures (Equation 2). The best fit to the experimental curves was obtained with Equation 2 with the following procedure: On differentiating Equation 2 it is easy to show that

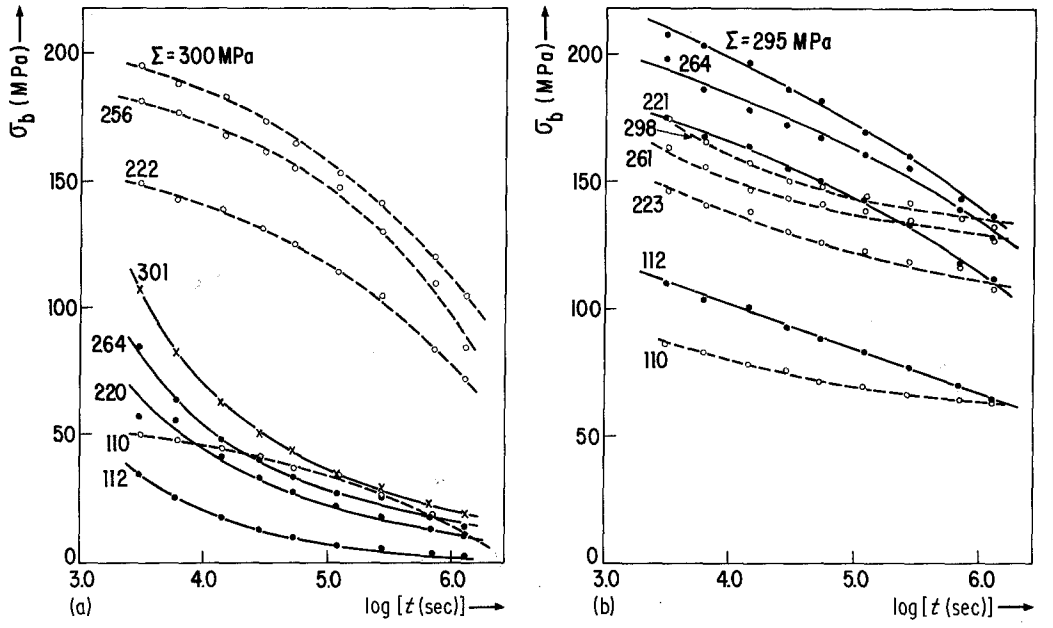

Figure 3 Measured stress change at the surface as a function of time for the AISI 304 specimens. (a) The full curves indicate specimens Type-A and the broken curves specimens Type-B, respectively. (b) The full curves are for specimens Type-C and the broken curves for specimens Type-D, respectively.

$$\nu = \lambda(\dot{\epsilon}^*/\dot{\epsilon})^{\lambda} \quad (16)$$

On combining Equations 2 and 16 leads to [27]

$$\ln \sigma = \ln \sigma - (\nu/\lambda) \quad (17)$$

Then, according to Equation 17 if the experimental curves are described by Equation 2 a plot of the natural logarithm of the stress against the derivative of the log σ–log $\dot{\epsilon}$ curves at this stress level should give a straight line of slope $1/\lambda$ and intercept ln σ. Once these parameters are known ϵ^* can be obtained from Equation 2. Equation 17 was applied to the experimental log σ–log $\dot{\epsilon}$ for Type-B and C specimens shown in Fig. 4 and the parameters obtained are given in Table VI. The experimental curves can be fitted with these parameters with a maximum error of 1%.

4. Discussion

4.1. A-286

As shown in Figs. 1 and 2, there are no substantial differences between the stress relaxation behaviour for specimens with treatments B, C or D. The cold-worked specimens (Type-A), however, show a stronger relaxation and the log σ–log $\dot{\epsilon}$ curves are concave upward, as compared with the linear behaviour shown by specimens Type-B, C or D. In all cases the stress relaxation curves are typical for a process occurring at low homologous tem-

TABLE V Parameters for the AISI 304 Type-A and D specimens, obtained by fitting the experimental log σ–log $\dot{\epsilon}$ curves of Fig. 4 to Johnston–Gilman equation

Specimen type	Σ (MPa)	$\sigma_i = 1/\alpha$ (MPa^{-1})	m^*	$\dot{\epsilon}^*/\sigma_i^{m^*} = \phi\rho b v_0/\sigma_0^{m^*}$ (sec^{-1} MPa$^{-m^*}$)	$(\dot{\epsilon}^*)^{1/m^*}\alpha$ (sec$^{-1/m^*}$ MPa^{-1})
A	301	46.4	5.4	4.5×10^{-18}	6.6×10^{-4}
	264	22.9	2.6	1.1×10^{-12}	2.1×10^{-5}
	220		4.6		3.4×10^{-4}
	112		3.3		1.4×10^{-4}
D	298	127	4.6	4.9×10^{-16}	4.7×10^{-4}
	261	116	6.5	3.4×10^{-19}	1.4×10^{-3}
	223	97.8	5.8	2.1×10^{-18}	8.7×10^{-4}
	110	50.8	7.0	1.6×10^{-19}	2.0×10^{-3}

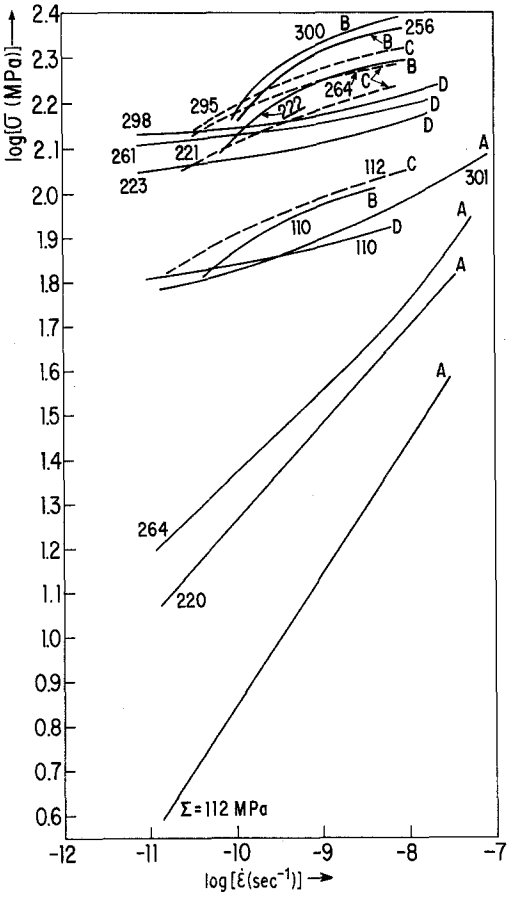

Figure 4 Stress against strain rate relaxation curves for the specimens of Fig. 3. The initial stresses and the thermomechanical treatment are indicated on each curve.

peratures [21], i.e. for mechanisms controlled by dislocation glide. Furthermore, as shown in Table III, m^* is constant for the stress relaxation curves obtained in the cold-worked specimens at different initial stresses. This might be an indication that the stress relaxation curves, for different Σ, are related by scaling, i.e. it is possible to superpose by translations ($\Delta \log \sigma$, $\Delta \log \dot{\epsilon}$) any one of the curves onto any of the others, in such a way that the overlapping segments of each curve match within the experimental error. The translations are performed along straight lines of slope, μ, given by [21]

$$\mu = \Delta \log \sigma / \Delta \log \dot{\epsilon} = \text{constant} \quad (18)$$

According to Povolo and Marzocca [28, 29] the scaling conditions for Equation 7 (or Equation 6) are

$$\Delta \log \beta = \Delta \log m^* = 0 \quad (19)$$

$$\Delta \log \sigma = -\Delta \log \alpha = \Delta \log \sigma_i \quad (20)$$

$$\Delta \log \dot{\epsilon} = \Delta \log \dot{\epsilon}^* = \Delta \log \sigma/\mu = \Delta \log \sigma_i/\mu \quad (21)$$

or

$$\alpha(\dot{\epsilon}^*)^\mu = \text{constant} \quad (22)$$

Then, if Equation 7 (or Equation 6) shows a scaling behaviour in a $\log \sigma$–$\log \dot{\epsilon}$ diagram m^* must be the same for all the individual stress relaxation curves at different Σ. Furthermore, if the mobile dislocation density remains constant during the relaxation [29]

$$\mu = 1/m^* \quad (23)$$

From the $\dot{\epsilon}^*$ and σ_i values obtained for the cold-worked specimens it can be seen that

$$\Delta \log \dot{\epsilon}^* = \Delta \log \sigma_i/2 \quad (24)$$

so that $\mu = 1/2 = 1/m^*$ and, according to the last column of Table III, Equation 22 is satisfied.

In summary, the stress relaxation curves for the cold-worked specimens are related by scaling along the translation path of slope $\mu = 1/2$ and the dislocation density remains constant during the relaxation. According to Table IV, $\alpha(\dot{\epsilon}^*)^{1/m^*}$ is practically independent from the initial stress and the thermomechanical treatment for specimens Type-B, C and D. There is a deviation at the lowest initial stress probably due to anelastic contributions. The dislocation density probably also remains constant during the relaxation, as for the cold-worked specimens.

If the mobile dislocation density does not change during the relaxation, the activation volume

$$V^* = -[\partial \Delta G/\partial(\sigma - \sigma_i)]_T \quad (25)$$

for Equation 6 is given by [30]

$$V^* = kTm^*/(\sigma - \sigma_i) \quad (26)$$

TABLE VI Parameters for the AISI 304 Type-B and C specimens, obtained by fitting the experimental $\log \sigma$–$\log \dot{\epsilon}$ curves of Fig. 4 to Equation 2

Specimen type	Σ (MPa)	$\sigma^* = 1/\alpha$ (MPa)	λ	$\dot{\epsilon}^*(\text{sec}^{-1})$
B	300	257.2	0.55	3.6×10^{-11}
	256	242.2	0.55	3.6×10^{-11}
	222	204	0.57	3.0×10^{-11}
	110	113	0.37	9.3×10^{-12}
C	295	248.8	0.13	2.0×10^{-11}
	264	226.5	0.09	1.6×10^{-11}
	221	345.5	0.23	3.6×10^{-12}
	112	171.9	0.22	5.4×10^{-12}

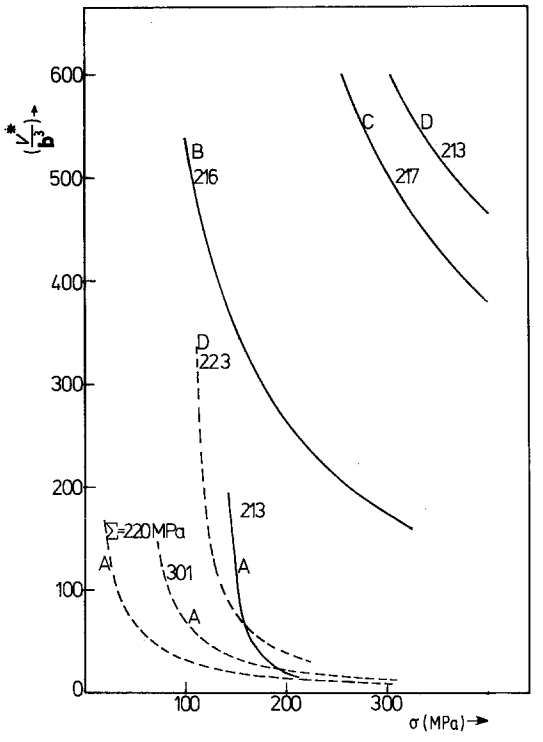

Figure 5 Relative activation volumes against stress, for different thermomechanical treatments. Full curves A-286 and broken curves AISI 304.

Furthermore, the activation work is

$$W = (\sigma - \sigma_i)V^* = m^*kT \qquad (27)$$

and

$$m^* = (\sigma - \sigma_i)V^*/kT \qquad (28)$$

According to Equation 28, m^* gives the ratio between the work of external forces and the thermal energy contribution to the overcoming of the obstacles by the moving dislocations [30].

The activation volumes calculated with Equation 26 and the parameters given in Tables III and IV are shown, as a function of stress, by the full curves of Fig. 5. Similar results are obtained for the rest of the initial stresses. It is seen that the activation volume is higher for specimens Type-B, C and D than for Type-A.

Since this alloy is a γ'-hardened austenitic steel [31] it is easy to rationalize the stress relaxation results. The ageing treatment at 993 K for specimens Type-B, C and D changes the distribution and size of the γ' particles. These specimens have high m^* values showing, according to Equation 28, that thermal activation is not important and the overcoming of the obstacles is mainly due to the work of external forces. This is also reflected in the high activation volumes obtained for these thermomechanical treatments. In the cold-worked specimens, which have not been aged, lower m^* values are obtained indicating smaller obstacles and a much stronger contribution of thermal activation. In addition, much smaller activation volumes are obtained, as shown in Fig. 5. In this case the mechanical behaviour is controlled by the overcoming of individual solutes or smaller precipitates by the moving dislocations.

Threadgill and Wilkshire [32] have studied the creep behaviour of a γ'-hardened austenitic steel at 873 K showing that the steady-state creep rate depends on the particle diameter and could be described by an equation similar to Equation 6.

4.2. AISI 304

As shown in Fig. 4, specimens Type-A and D give concave upward $\log \sigma$–$\log \dot{\epsilon}$ curves that can be described by Equation 6. Furthermore, as shown in Table V, m^* and $\alpha(\dot{\epsilon}^*)^{1/m^*}$ depend on the initial stress showing that Σ affects the mobile dislocation density and no scaling behaviour is found between the individual stress relaxation curves. If the mobile dislocation density is assumed to remain constant during an individual stress relaxation at a given Σ, Equation 26 can be used to calculate the activation volume. The results are shown by the broken curves of Fig. 5. It is seen that, in general, much smaller activation volumes than for the A-286 specimens are obtained, for the same initial stress and thermomechanical treatment.

According to Fig. 5, the activation volumes for the cold-worked specimens are higher, at a given stress, than those for the A-286 cold-worked specimens but they tend to be the same at high stresses. The shifting of the curves to lower stresses, for the A-286 specimens, is due to the higher internal stresses found in this alloy, as shown by a comparison between Tables III and V. The m^* values for AISI 304 are slightly higher than for A-286 even if of the same order of magnitude. These low m^* values indicate that thermal activation is important. It can be concluded that the stress relaxation behaviour of the AISI 304 cold-worked specimens is controlled by a mechanism similar to the one found in the A-286 cold-worked specimens, i.e. the overcoming of individual solute atoms or very small precipitates. The smaller

relaxation found in the A-286 alloy is due to the higher internal stresses.

As shown by Table V, specimens Type-D give m^* values similar to those found for the cold-worked specimens. As indicated by the activation volumes shown in Fig. 5 a similar mechanism as for the cold-worked specimens is controlling the stress–relaxation behaviour. The lower relaxation for Type-D specimens is due to the higher internal stresses after this type of thermomechanical treatment.

Remarkable results are obtained for the stress relaxation of Type-B and C specimens. In fact, as shown by Fig. 4, the stress relaxation $\log \sigma - \log \dot{\epsilon}$ curves are concave downward, typical for processes occurring at high homologous temperatures [21]. It was shown that the relaxation behaviour of these specimens can be very well described by Hart's equation for high homologous temperatures (Equation 2) with the parameters given in Table VI. The problem with Equation 2 is that it is only phenomenological and it is difficult to attach a physical significance to the parameters involved.

As pointed out in Section 1, Rhode and Swearengen [2] have proposed Equation 1 to describe stress relaxation concurrent with microstructural recovery. Equation 6 is a particular case of Equation 1 when no recovery occurs. Since, as shown by Swearengen and Rhode [33], Equation 1 can give either concave upward, linear or concave downward curves, it was attempted to fit the stress relaxation curves for Type-B and C specimens to this equation. In fact, Equation 1 can be written, in normalized form, as

$$\dot{\epsilon}/\dot{\epsilon}^* = [\beta(\alpha\sigma - 1)^{m/n} + (\alpha\sigma - 1)]^n \quad (29)$$

where

$$\dot{\epsilon}^* = \dot{\epsilon}_1(\sigma_i/\sigma_1)^n A^n \quad (30)$$

$$\beta = [(1-A)/A](\sigma_i/\sigma_1)^{m/n-1} \quad (31)$$

$$\alpha = 1/\sigma_i \quad (32)$$

By differentiating Equation 29 it is easy to show that the strain rate sensitivity parameter, in this case, is given by

$$\nu = \frac{n\alpha\sigma}{(\alpha\sigma - 1)} \times \left[\frac{m}{n}\beta(\alpha\sigma - 1)^{m/n-1} + 1\right] \Big/ [\beta(\alpha\sigma - 1)^{m/n-1} + 1] \quad (33)$$

On combining Equations 29 and 33 leads to

$$\frac{\nu(\alpha\sigma - 1)}{\alpha\sigma} = m + (n-m)(\dot{\epsilon}^*)^{1/n}\frac{(\alpha\sigma - 1)}{\dot{\epsilon}^{1/n}} \quad (34)$$

In addition, if $\alpha\sigma \gg 1$, i.e. if $\sigma \gg \sigma_i$ Equation 34 reduces to

$$\nu = m + (n-m)(\dot{\epsilon}^*)^{1/n}\alpha\frac{\sigma}{\dot{\epsilon}^{1/n}} \quad (35)$$

and Equation 29 to

$$\frac{\dot{\epsilon}^{1/n}}{\sigma} = \beta(\dot{\epsilon}^*)^{1/n}\alpha^{m/n}\sigma^{m/n-1} + \alpha(\dot{\epsilon}^*)^{1/n} \quad (36)$$

Then, when $\alpha\sigma \gg 1$, Equation 35 shows that a plot of ν against $\sigma/\dot{\epsilon}^{1/n}$ should give a straight line of slope $(n-m)(\dot{\epsilon}^*)^{1/n}$ and intercept m; Equation 36 that a plot of $\dot{\epsilon}^{1/n}/\sigma$ against $\sigma^{m/n-1}$ should give a straight line of slope $\beta(\dot{\epsilon}^*)^{1/n}\alpha^{m/n}$ and intercept $\alpha(\dot{\epsilon}^*)^{1/n}$. Only the parameter n is required to use Equation 35 for the experimental data; both n and m are needed for Equation 36.

Equations 35 and 36 were used for the experimental $\log \sigma - \log \dot{\epsilon}$ curves for Type-B and C specimens, shown in Fig. 4. n was obtained, as suggested in [33], from the reciprocal of the slope of the curves at low stresses; similarly, m can be obtained from the reciprocal of the slopes at high stresses. This procedure gives, for example, for the curve at $\Sigma = 300$ MPa for specimen Type-B, $n = 3.4$ and $m = 17$. The plots suggested by Equations 35 and 36 show strong curvatures, for both Type-B and C specimens, indicating either that Equation 29 (or Equation 1) is not obeyed or that wrong values have been chosen for n or, that the condition $\alpha\sigma \gg 1$ is not satisfied. In this situation it is difficult to determine all the parameters needed for Equation 1.

A possible interpretation for the change in the curvature of the relaxation curves for specimens Type-B and C can be obtained by an analysis of Equations 2 and 6 in terms of a general equation that describes thermally activated dislocation motion. This very well known equation leads to

$$\dot{\epsilon} = \dot{\epsilon}_0 \exp[-\Delta G(\sigma - \sigma_i)/kT] \quad (37)$$

where $\dot{\epsilon}_0$ is a general pre-exponential factor. Equation 2 can be written in the form of Equation 37 as

$$\dot{\epsilon} = \dot{\epsilon}^* \exp\left\{-\frac{1}{\lambda}\ln[\ln(\sigma^*/\sigma)]\right\} \quad (38)$$

so that

$$\Delta G(\sigma - \sigma_i) = \frac{1}{\lambda} \ln [\ln(\sigma^*/\sigma)] kT \quad (39)$$

It is easy to show that Equation 2 reduces to Equation 6 if

$$\sigma_i = \sigma - \sigma_0 [\ln(\sigma^*/\sigma)]^{-1/\lambda m^*} \quad (40)$$

$$\dot{\epsilon}^* = \phi \rho \mathbf{b} v_0 \quad (41)$$

and the mobile dislocation density does not depend on the applied stress.

Then, Equation 2 is equivalent to Equation 6 if the internal stress changes according to Equation 40 during the relaxation and $\dot{\epsilon}^*$ is given by Equation 41. As shown in Table VI, $\dot{\epsilon}^*$ has the correct order of magnitude. On taking into account Equations 25, 39 and 40 it is easy to show that the activation volume is given, in this case, by

$$V^* = \frac{m^* kT}{\sigma_0} [\ln(\sigma^*/\sigma)]^{1/\lambda m^*} \quad (42)$$

According to this equation, unfortunately, the parameters σ_0 and m^* are needed to calculate the activation volume for specimens Type-B and C. A comparison with the results obtained in Type-A and D specimens, however, can be made by the following procedure: On differentiating Equation 42 it is easy to show that

$$m^*(\mathrm{d} \log V^*/\mathrm{d} \log \sigma) = -\frac{1}{\lambda} [\ln(\sigma^*/\sigma)]^{-1} \quad (43)$$

and, on differentiating Equation 6 leads to

$$m^*(\mathrm{d} \log V^*/\mathrm{d} \log \sigma) = -\sigma m^*/(\sigma - \sigma_i) \quad (44)$$

Then, Equations 43 and 44 shows that the results obtained for specimens Type-B and C can be compared with those for specimens Type-A and D through the parameter m^* (d log V^*/d log σ). The results obtained, for similar initial stresses and with the parameters given in Tables V and VI, are shown in Fig. 6. Furthermore, as shown by Fig. 7 both σ_i and σ^* change linearly with the initial stress, except for specimens Type-C where some dispersion is observed.

In summary, it may be stated that the different behaviour found for specimens Type-B and C with respect to specimens Type-A and D might be due to the fact that the microstructure is changing during the relaxation in the first type of specimens, but the same mechanism is controlling the plastic deformation.

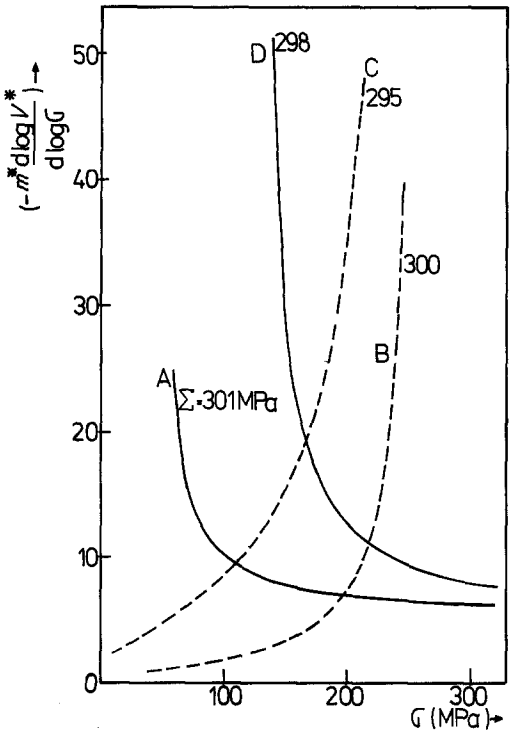

Figure 6 Parameter $-m^*(\mathrm{d} \log V^*/\mathrm{d} \log \sigma)$ given either by Equation 43 or Equation 44 against stress, for AISI 304.

Unfortunately, only few detailed studies of the changes in the microstructure due to different thermomechanical treatments have been reported in the literature. In addition, scarce experiments where a correlation is established between the mechanical behaviour and the microstructure have

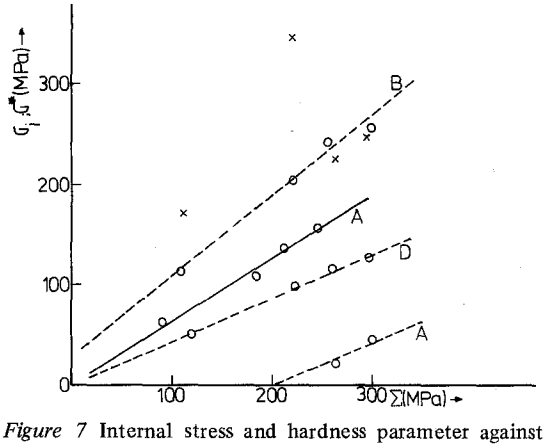

Figure 7 Internal stress and hardness parameter against initial stress. Broken lines AISI 304 and full lines A-286. The dots correspond to AISI 304 Type-C specimens. The type of specimen is indicated on each curve.

been performed, and generally at temperatures higher than the one used in this paper.

The difference in the stress relaxation behaviour induced by the different thermomechanical treatments might come from a different distribution of the precipitates. In fact, Cole *et al.* [34] have shown that the phases formed and the location of the carbides depend on the time and temperature chosen either for the solution annealing, for the solution annealing and carbide agglomeration or for the ageing treatment. Furthermore, Yang and Spruiell [35] have studied the recovery stages of cold-worked type 304 stainless steels. Isochronal annealing revealed a distinguishable stage of resistivity recovery prior to recrystallization, which was attributed to the annihilation of vacancies and removal of carbon from solid solution. A second stage resistivity drop (around 773 K) resulted from recrystallization.

From the stress relaxation results reported by Anciaux [4], at 563 K, for mill-annealed type 304 stainless steel, changes in the concavity of the $\log \sigma - \log \dot{\epsilon}$ curves are observed, depending on the prestraining before the relaxation. According to the data reported by Thomas and Yaggee [8], for 20% cold-worked type 316 steel, a change in the concavity of the stress relaxation curves is observed even at room temperature. These would indicate that recovery could occur at 563 K and possibly at room temperature, which is not easy to understand even if it is known that carbon begins to be trapped by vacancies near room temperature [36, 37].

Another possibility is that grain-boundary sliding contributes to the stress relaxation for certain thermomechanical treatments. In fact, as pointed out in Section 1, Huang *et al.* [14] have observed such a contribution at 873 K, in highly stabilized type 316 stainless steel. A grain-boundary sliding contribution to the stress relaxation is possible at 773 K but it is difficult to rationalize how this effect can be important at 563 K and at room temperature. Finally, as shown by the grain sizes and the microhardness values given in Table II there is no clear correlation between these quantities and the stress relaxation behaviour.

In conclusion, further work is needed for a correct understanding of the mechanisms controlling the stress relaxation behaviour of AISI 304. Particularly, the meaning of the parameters and the barriers involved, if the simple model used in this paper is valid, should be established.

5. Conclusions

The relaxation of Type AISI 304 and A-286 steels at 773 K depends strongly on the thermomechanical treatment given to the specimens prior to the stress relaxation testing. The data were interpreted in terms of a stress-partitioned power law and it was shown, for AISI 304, that, for certain thermomechanical treatments, the internal stress is dependent on the applied stress since the microstructure recovers during the relaxation.

Acknowledgements

We wish to express our appreciation to Lic. J. C. Crespi for his helpful comments.

This work was performed within the Special Intergovernmental Agreement Between Argentina and the Federal Republic of Germany and was supported partially by the "Proyecto Multinacional de Tecnología de Materiales" OAS-CNEA and the CIC.

References

1. J. N. CONWAY, R. H. STENTZ and J. T. BERLING, Fatigue, Tensile, and Relaxation Behaviour of Stainless Steels, USAEC Report TID-26135 (1975).
2. R. W. ROHDE and J. C. SWEARENGEN, Transactions of the 4th International Conference on Structural Mechanics in Reactor Technology, edited by A. Jaeger and B. A. Boley (North-Holland, Amsterdam, 1977) Vol. L,p. L8/5.
3. J. B. CONWAY, An analysis of the Relaxation Behaviour of AISI 304 and 316 Stainless Steel at Elevated Temperature, USAEC Report GEMP-730, General Electric Company (1969).
4. M. J. ANCIAUX, *Metall. Trans.* **12A** (1981) 1981.
5. E. W. HART, *Trans. J. Eng. Mater. Technol.* 98 (1976) 193.
6. *Idem*, Transactions of the 4th International Conference on Structural Mechanics in Reactor Technology, edited by A. Jaeger and B. A. Boley (North-Holland, Amsterdam, 1977) Vol. L,p. L1/1*.
7. H. YAMADA and CHE-YU LI, *Metall. Trans.* 4 (1973) 2133.
8. J. F. THOMAS Jr and F. L. YAGGEE, *ibid.* **6A** (1975) 1835.
9. G. L. WIRE, F. V. ELLIS and CHE-YU LI, *Acta Metall.* 24 (1976) 677.
10. CHE-YU LI, F. V. ELLIS and F. H. HUANG, "Alloys and Microstructural Design", edited by J. K. Tien and G. S. Ansell (Academic Press, New York, 1976) p. 403.
11. N. NIR, F. H. HUANG, E. W. HART and CHE-YU LI, *Metall. Trans.* **8A** (1977) 583.

12. F. H. HUANG, F. V. ELLIS and CHE-YU LI, *Metall. Trans.* 8A (1977) 699.
13. Y. YAMADA, *Scripta Metall.* 11 (1977) 321.
14. F. H. HUANG, H. YAMADA and CHE-YU LI, Proceedings of the V International Conference on Materials Technology, Sao Paulo (1978) p. 83.
15. R. G. MATTERS and R. E. LOCHEN, *Proc. ASTM* 56 (1956) 672.
16. D. E. FRASER, P. A. ROSS-ROSS and A. R. CAUSEY, *J. Nucl. Mater.* 46 (1973) 281.
17. F. POVOLO and E. H. TOSCANO, *J. Nucl. Mater.* 74 (1978) 76.
18. F. POVOLO and E. H. TOSCANO, *ibid.* 78 (1978) 217.
19. L. D. BLACKBURN, The Generation of Isochronous Stress Strain Curves, ASME Winter Annual Meeting, New York, November 1972 (ASME, New York).
20. Röchling'sche Eisen -und Stahlwerke GmbH, Handbuch für hochwarmfeste Stähle und Legienrungen (Völklingen, Germany) p. 49.
21. E. W. HART, CHE-YU LI, H. YAMADA and G. L. WIRE, "Constitutive Equations in Plasticity", edited by A. S. Argon (MIT Press, Cambridge, 1975) p. 149.
22. F. POVOLO, *J. Nucl. Mater.* 96 (1981) 178.
23. J. J. GILMAN, *Austral. J. Phys.* 13 (1960) 327.
24. W. G. JOHNSTON and J. J. GILMAN, *J. Appl. Phys.* 30 (1959) 139.
25. F. POVOLO, Proceedings of the XXXVIII Congresso Anual Associação Brasíleíra de Matais Vol. 3 (ABM, São Paulo, 1983) p. 263.
26. A. W. SLEESWYK, G. H. BOERSMA, G. HUNT and D. J. VEREL, Proceedings of the 2nd International Conference on Strength of Metals and Alloys, Vol. I (ASM, Ohio, 1976) p. 204.
27. F. POVOLO and M. HIGA, *J. Nucl. Mater.* 91 (1980) 189.
28. F. POVOLO and A. J. MARZOCCA, *J. Mater. Sci.* 18 (1983) 1426.
29. *Idem, Trans. Jpn. Inst. Met.* 24 (1983) 111.
30. V. I. DOTSENKO, *Phys. Status Solidi (b)* 93 (1979) 11.
31. J. GORDON PARR and A. HANSON, "An Introduction to Stainless Steels" (American Society for Metals, Ohio, 1965).
32. P. L. THREADGILL and B. WILKSHIRE, "Creep Strength in Steels and High Temperature Alloys" (The Metals Society, London, 1974) p. 8.
33. J. C. SWEARENGEN and R. W. RHODE, *Met. Trans.* 8A (1977) 577.
34. N. C. COLE, G. M. GOODWIN and G. M. SLAUGHTER, "Microstructural Science", Vol. 3, edited by P. M. French, R. Gray and J. L. McCall (American Elsevier, 1975) p. 789.
35. S. W. YANG and J. E. SPRUIELL, *J. Mater. Sci.* 17 (1982) 677.
36. M. S. ANAND, B. M. PANDE and R. P. AGARWALA, *J. Nucl. Mater.* 58 (1975) 117.
37. F. E. FUJITA and A. C. DAMASK, *Acta Metall.* 12 (1964) 331.

Received 26 January
and accepted 21 September 1983